# Comparing pathways for electricity-based production of dimethoxymethane as a sustainable fuel – Supplementary Information

Jannik Burre,[a] Dominik Bongartz,[a] Sarah Deutz,[d] Chalachew Mebrahtu,[f] Ole Osterthun,[f] Ruiyan Sun,[f] Simon Völker,[d] André Bardow,[b,c,d,e] Jürgen Klankermayer,[f] Regina Palkovits,[f] and Alexander Mitsos*,[b,a,c]

[a]Process Systems Engineering (AVT.SVT), RWTH Aachen University, Forckenbeckstraße 51, 52074 Aachen, Germany.

[b]JARA-ENERGY, 52056 Aachen, Templergraben 55, Germany.

[c]Institute of Energy and Climate Research: Energy Systems Engineering (IEK-10), Forschungszentrum Jülich GmbH, Wilhelm-Johnen-Straße, 52425 Jülich, Germany.

[d]Institute of Technical Thermodynamics, RWTH Aachen University, Schinkelstraße 8, 52062 Aachen, Germany.

[e]Department of Mechanical and Process Engineering, ETH Zurich, Tannenstraße 3, 8092 Zurich, Switzerland.

[f]Institute of Technical and Macromolecular Chemistry, RWTH Aachen University, Worringerweg 1, 52074 Aachen, Germany.

April 26, 2021

# 1 Dimethoxymethane synthesis

## 1.1 Process concept for the established pathway

On the basis of Reaction (R1), established process concepts utilize a fixed-bed reactor with an acidic ion exchange resin (Amberlyst 15) as catalyst.[1] A reaction temperature of about 60 °C, a pressure just higher than ambient pressure to avoid substrate evaporation (e.g., 2 bar), and methanol in excess enable almost perfect selectivity toward dimethoxymethane (DMM) at almost complete FA conversion. Product separation is achieved by a two-pressure distillation to break the azeotrope between methanol and DMM. The first distillation column additionally contains a reactive section for converting leftover FA and a vapor side draw for removing excess methanol. Methanol can be produced from $H_2$ and $CO_2$ via Reaction (R2) with catalysts based on those for methanol formation from syngas ($H_2$ and carbon monoxide (CO)).[2–4] Alternatively, methanol can be obtained from syngas,[5] which in turn can be produced via the reverse water gas shift reaction from $H_2$ and $CO_2$. FA is produced from methanol either via partial oxidation over an iron, molybdenum, or vanadium oxide catalyst or via combined partial oxidation and dehydrogenation over a silver catalyst (Reaction (R3)).[6] In the latter case, the formed $H_2$ is diluted in the off-gas of the absorption column and is burned for energy recovery. Formaldehyde is removed from the gaseous product mixture via absorption in water.

## 1.2 Oxidation of methanol

For the direct oxidation of methanol to DMM (Reaction (R5)), a gaseous substrate mixture of methanol and an oxidant (typically air) is fed into a fixed-bed reactor. The reactor is operated continuously under atmospheric pressure at temperatures between 120 °C and 240 °C and gas hourly space velocities (GHSV) between $10.000\,\mathrm{mL\,h^{-1}\,g_{cat}^{-1}}$ and $40.000\,\mathrm{mL\,h^{-1}\,g_{cat}^{-1}}$.[7] To ensure safe operation, the applied methanol concentration should stay outside of the explosive range (7 % to 36 % in air).

Extensive research on the direct oxidation of methanol toward DMM has resulted in a large number of bifunctional catalysts comprising redox and acidic active sites. The bifunctional nature of such catalysts plays a key role in directing the reaction network toward the selective formation of DMM. An appropriate ratio between redox and acidic properties is crucial for high DMM selectivities (80 % to 99 %[7]). Among the reported catalysts, silicia-modified and $TiO_2$-supported vanadium oxide (VTiSi) features a state-of-the-art performance with an DMM selectivity of up to 99 % at a methanol conversion of 51 % and a reaction temperature of 140 °C (ESI Tab. S1).[8]

## 1.3 Reduction of $CO_2$

The resource-efficient reduction of $CO_2$ toward DMM (Reaction (R6)) is enabled by a homogeneous ruthenium-based catalyst, which is dissolved together with a co-catalyst into a liquid methanol solution. Under high pressure (80 bar) and high temperature (80 °C), turnover numbers (the amount of substrate molecules converted into product molecules per active catalyst site, TON) of up to 214 toward DMM could be achieved.[9] Schieweck and Klankermayer[10] later exchanged the ruthenium-based catalyst by an earth abundant cobalt catalyst to perform the same reaction. A study by Siebert *et al.*[11] revealed further potential of the ruthenium system: By using a Design of Experiments approach, a TON of 786 for DMM could be achieved. Although TON and yield (product of selectivity and conversion) correlate linearly for a fixed catalyst concentration, a high TON does not necessarily mean a high yield. For low catalyst concentrations, product yield can be low although the TON of the catalyst is high. For industrial implementation, achieving a reasonable high DMM yield is key—preferably with only a small amount of catalyst thus high TON. For the reduction of $CO_2$ toward DMM, a maximum yield of 8.3 % (selectivity of 81.8 %, conversion of 10.8 %) has been achieved (ESI Tab. S1).

## 1.4 Dehydrogenation of methanol

The dehydrogenation of methanol (Reaction (R8)) proceeds in a gas-phase fixed-bed reactor in the presence of a tailored Cu/Hß bifunctional catalyst. A high $SiO_2$-to-$Al_2O_3$ ratio (836) of the zeolite Hß ensures a high selectivity toward DMM (up to 80.3 %) at a conversion of 3.6 %.[12] This is possible even at mild reaction conditions due to the coupling of methanol dehydrogenation and FA acetalization. Temperatures at around 200 °C, atmospheric pressure, and a GHSV of 14.549 $mL\,h^{-1}\,g_{cat}^{-1}$ are sufficient (ESI Tab. S1).

## 1.5 Transfer-hydrogenation of methanol

The transfer-hydrogenation of methanol (Reaction (R9)) was published recently by Osterthun and Klankermayer[13] and requires the presence of a homogeneous iridium catalyst and the presence of a Lewis acid. TONs up to 204 for DMM could be achieved for a system at 100 °C and 20 bar. A selectivity as high as 98.2 % at a methanol conversion of 0.9 % could be achieved so far (ESI Tab. S1).

Table S1: Reaction parameters of the experiments with the highest reported yields for DMM synthesis via different routes. Abbreviations: VTiSi = silica-modified and titanium-oxide-supported vanadium oxide, Ru(triphos)(tmm) = triphos-based ruthenium catalyst, Cu/Hß = Hß zeolite with copper nanoparticles, Ir(DPEphos)(cod) = Bis[(2-diphenylphosphino)phenyl]ether-based iridium catalyst, Het. = Heterogeneous, Hom. = Homogeneous, conc. = concentration

| Parameter | Established[1,14] (Reaction (R1)) | Oxidative[7,8] (Reaction (R5)) | Reductive[9] (Reaction (R6)) | Dehydrogenative[12] (Reaction (R8)) | Transfer-hydrogenative[13] (Reaction (R9)) |
|---|---|---|---|---|---|
| Catalyst [-] | Amberlyst 15 | VTiSi | Ru(triphos)(tmm) | Cu/Hß | Ir(DPEphos)(cod) |
| Phase [-] | Het. | Het. | Hom. | Het. | Hom. |
| Temperature [°C] | 60 | 140 | 80 | 200 | 100 |
| Pressure [bar] | 2 | 1 | 80 | 1 | 20 |
| Residence time [h] | 0.2 | N/A | 18 | N/A | 18 |
| GHSV [$\mathrm{mL\,h^{-1}\,g_{cat}^{-1}}$] | N/A | 12,000 | N/A | 14,549 | N/A |
| Catalyst conc. [$\mathrm{mmol\,L^{-1}}$] | N/A | N/A | 12.5 | N/A | 0.25 |
| Methanol conversion [%] | 12.8 | 51.0 | 10.1 | 3.6 | 0.9 |
| DMM selectivity [%] | 99.9 | 99.0 | 81.8 | 80.3 | 98.2 |

# 2 Thermodynamic model parameters

Pure component property data is taken from the Aspen Plus v11 databank APV110 PURE37. Parameters for the UNIFAC model for the established pathway are taken from Fredenslund *et al.*[15], Maurer[16], Hasse *et al.*[17], Hahnenstein *et al.*[18], Albert *et al.*[19],[20],[21], and Kuhnert *et al.*[22]. Parameters for the NRTL model for the direct pathways are given in ESI Tab. S2-S4.

Table S2: NRTL parameter $a_{ij}$ (Aspen Plus notation) for nonideal interactions within the multi-component system of the direct pathways. The remaining interactions are assumed to be ideal

| | Component j | | | | | |
|---|---|---|---|---|---|---|
| Component i | Water | DMM | MeOH | MF | DME | $CO_2$ |
| Water | N/A | 0[a] | 2.7322[a] | −91.5425[d] | 0.825228[b] | 10.064[e] |
| DMM | 0[a] | N/A | 0[a] | −0.359076[d] | 0[c] | 0 |
| MeOH | −0.693[a] | 0[a] | N/A | 0[a] | 8.0627[b] | 0 |
| MF | −86.3908[d] | 0.224382[d] | 0[a] | N/A | 0.224382[g] | 0 |
| DME | 0.96683[b] | 0[c] | −15.0667[b] | −0.359076[g] | N/A | 0.394439[f] |
| $CO_2$ | 10.064[e] | 0 | 0 | 0 | −0.44005[f] | N/A |

[a] From AspenPlus APV110 VLE-IG databank.
[b] From Dirk-Faitakis *et al.*[23].
[c] From Breitkreuz *et al.*[24].
[d] From Deutz *et al.*[25].
[e] From AspenPlus APV110 ENRTL-RK databank.
[f] From NISTV84 NIST-HOC databank.
[g] In accordance to the assumptions in Breitkreuz *et al.*[24].

Table S3: NRTL parameter $b_{ij}$ (Aspen Plus notation) for nonideal interactions within the multi-component system of the direct pathways. The remaining interactions are assumed to be ideal

| | Component j | | | | | |
|---|---|---|---|---|---|---|
| Component i | Water | DMM | MeOH | MF | DME | $CO_2$ |
| Water | N/A | 618.9311[a] | −617.2687[a] | 13650[d] | 65.5774[b] | −3268.135[e] |
| DMM | 491.2114[a] | N/A | 175.4218[a] | 100[d] | 0[c] | 0 |
| MeOH | 172.9871[a] | 303.1328[a] | N/A | 199.0137[a] | −1659.63[b] | 0 |
| MF | 15500[d] | 0[d] | 217.046[a] | N/A | 0[g] | 0 |
| DME | −39.5507[b] | 0[c] | 3836.09[b] | 100[g] | N/A | 0[f] |
| $CO_2$ | −3268.135[e] | 0 | 0 | 0 | 0[f] | N/A |

[a] From AspenPlus APV110 VLE-IG databank.
[b] From Dirk-Faitakis *et al.*[23].
[c] From Breitkreuz *et al.*[24].
[d] From Deutz *et al.*[25].
[e] From AspenPlus APV110 ENRTL-RK databank.
[f] From NISTV84 NIST-HOC databank.
[g] In accordance to the assumptions in Breitkreuz *et al.*[24].

Table S4: NRTL parameter $c_{ij}$ (Aspen Plus notation) for nonideal interactions within the multi-component system of the direct pathways. The remaining interactions are assumed to be ideal

| | Component j | | | | | |
|---|---|---|---|---|---|---|
| Component i | Water | DMM | MeOH | MF | DME | $CO_2$ |
| Water | N/A | 0.3[a] | 0.3[a] | 0.383[d] | −0.77735[b] | 0.2[e] |
| DMM | 0.3[a] | N/A | 0.3[a] | 0.3[d] | 0[c] | 0 |
| MeOH | 0.3[a] | 0.3[a] | N/A | 0.3[a] | −0.12748[b] | 0 |
| MF | 0.383[d] | 0.3[d] | 0.3[a] | N/A | 0.3[g] | 0 |
| DME | −0.77735[b] | 0[c] | −0.12748[b] | 0.3[g] | N/A | 0.5[f] |
| $CO_2$ | 0.2[e] | 0 | 0 | 0 | 0.5[f] | N/A |

[a] From AspenPlus APV110 VLE-IG databank.
[b] From Dirk-Faitakis *et al.*[23].
[c] From Breitkreuz *et al.*[24].
[d] Additionally, $f_{H_2O,MF} = 0.1613$ and $f_{MF,H_2O} = 0.1219$ need to be provided. From Deutz *et al.*[25].
[e] From AspenPlus APV110 ENRTL-RK databank.
[f] From NISTV84 NIST-HOC databank.
[g] In accordance to the assumptions in Breitkreuz *et al.*[24].

# 3 Model equations and assumptions for pathway evaluation

Table S5: Level-specific input data for DMM pathway evaluation. $\dot{E}_{\mathrm{H_2}}$, $\dot{E}_{\mathrm{CO_2}}$, $\dot{E}_{\mathrm{DMM}}$, and $\dot{E}_{\mathrm{side}}$ is the DMM-specific thermomechanical and chemical (based on higher heating value) exergy content of $H_2$, $CO_2$, DMM, and side products respectively; $\dot{E}_{\dot{\mathrm{Q}}}$ is the DMM-specific exergy demand of the process ($T_{\mathrm{ambient}} = 298.15\mathrm{K}$); $P_{\mathrm{feed}}$ and $P_{\mathrm{misc}}$ is the DMM-specific electricity demand for feed compression and miscellaneous compression and pumping within the entire process, respectively; $I_{\mathrm{H_2}}$, $I_{\mathrm{CO_2}}$, $I_{\mathrm{comb}}$, $I_{\mathrm{side}}$, $I_{\mathrm{steam}}$, $I_{\mathrm{coolant}}$, $I_{\mathrm{P,feed}}$, and $I_{\mathrm{P,misc}}$ is the impact on climate change contribution resulting from $H_2$ supply, $CO_2$ supply, fuel combustion, side product treatment, steam demand, cooling demand, feed compression, and miscellaneous compression and pumping, respectively; $C_{\mathrm{H_2}}$, $C_{\mathrm{CO_2}}$, $C_{\mathrm{steam}}$, $C_{\mathrm{coolant}}$, $C_{\mathrm{P,feed}}$, $C_{\mathrm{P,misc}}$, $C_{\mathrm{inv}}$, and $C_{\mathrm{misc}}$ is the production cost contribution resulting from $H_2$ supply, $CO_2$ supply, steam demand, cooling demand, feed compression, miscellaneous compression and pumping, investment cost, and miscellaneous costs, respectively

| Level | Input variables | | | | | | | | | | | | | | | | | | | | | |
|---|---|---|---|---|---|---|---|---|---|---|---|---|---|---|---|---|---|---|---|---|---|---|
| | Efficiency | | | | | | | Impact on climate change | | | | | | | | | | Cost | | | | |
| | $\dot{E}_{\mathrm{H_2}}$ | $\dot{E}_{\mathrm{CO_2}}$ | $\dot{E}_{\mathrm{DMM}}$ | $\dot{E}_{\mathrm{side}}$ | $\dot{E}_{\dot{\mathrm{Q}}}$ | $P_{\mathrm{feed}}$ | $P_{\mathrm{misc}}$ | $I_{\mathrm{H_2}}$ | $I_{\mathrm{CO_2}}$ | $I_{\mathrm{comb}}$ | $I_{\mathrm{side}}$ | $I_{\mathrm{steam}}$ | $I_{\mathrm{coolant}}$ | $I_{\mathrm{P,feed}}$ | $I_{\mathrm{P,misc}}$ | $C_{\mathrm{H_2}}$ | $C_{\mathrm{CO_2}}$ | $C_{\mathrm{steam}}$ | $C_{\mathrm{coolant}}$ | $C_{\mathrm{P,feed}}$ | $C_{\mathrm{P,misc}}$ | $C_{\mathrm{inv}}$ | $C_{\mathrm{misc}}$ |
| 1 | X | X | X | | | | | X | X | X | | | | | | X | X | | | | | |
| 2 | X | X | X | X | X | X | | X | X | X | X | X | X | X | | X | X | X | X | X | | |
| 3 | X | X | X | X | X | X | X | X | X | X | X | X | X | X | X | X | X | X | X | X | X | X |

The DMM-specific minimum raw material consumption $m_{\mathrm{L1,i}}$ on Level 1 is calculated according to ESI Equation (1):

$$m_{\mathrm{L1,i}} = \frac{|\nu_{\mathrm{i}}|}{\nu_{\mathrm{DMM}}} \frac{M_{\mathrm{i}}}{M_{\mathrm{DMM}}} \qquad \mathrm{i} \in \{\mathrm{H_2}, \mathrm{CO_2}\}, \tag{1}$$

with the stoichiometric coefficients of the overall reaction equation towards DMM, $\nu_{\mathrm{i}}$ and $\nu_{\mathrm{DMM}}$, and the molar mass of component i and DMM, $M_{\mathrm{i}}$ and $M_{\mathrm{DMM}}$ , respectively.

## 3.1 Exergy efficiency

System exergy efficiency $\eta_{\mathrm{S,l}}$ is calculated by

$$\eta_{\mathrm{S,l}} = \frac{\dot{E}_{\mathrm{DMM}} + \dot{E}_{\mathrm{side}} + \dot{E}_{\dot{\mathrm{Q}}_{\mathrm{out}}}}{m_{\mathrm{l,H_2}} B_{\mathrm{H_2}} + m_{\mathrm{l,CO_2}} B_{\mathrm{CO_2}} + \dot{E}_{\dot{\mathrm{Q}}_{\mathrm{in}}} + P_{\mathrm{feed}} + P_{\mathrm{misc}}} \qquad \mathrm{l} \in \{\mathrm{L1}, \mathrm{L2}, \mathrm{L3}\}, \tag{2}$$

where $\dot{E}_{\mathrm{DMM}}$ and $\dot{E}_{\mathrm{side}}$ is the DMM-specific thermomechanical and chemical (based on higher heating value) exergy content of DMM and side products , respectively; $\dot{E}_{\dot{\mathrm{Q}}_{\mathrm{out}}}$ and $\dot{E}_{\dot{\mathrm{Q}}_{\mathrm{in}}}$ is the DMM-specific exergy of excess heat and heat demand of the process, respectively ($T_{\mathrm{ambient}} = 298.15\mathrm{K}$); $B_{\mathrm{H_2}}$ and $B_{\mathrm{CO_2}}$ is the $H_2$- and $CO_2$-specific exergy demand for producing $H_2$ and capturing $CO_2$, respectively; $P_{\mathrm{feed}}$ and $P_{\mathrm{misc}}$ is the DMM-specific electricity demand for feed compression and miscellaneous compression and pumping within the entire process, respectively.

## 3.2 Sizing and costing

The column diameter $D_{\mathrm{col}}$ is determined by the molar vapor flow $\dot{V}$ such that tray flooding is prevented in the highest loaded column section. The column diameter $D_{\mathrm{col}}$ is calculated according to ESI Equation (3):

$$D_{\mathrm{col}} = \sqrt{\frac{1}{F_{\mathrm{v}}(1-\phi)} \frac{4}{\pi} \frac{\dot{V}}{n_{\mathrm{col}}} \sqrt{\frac{R T_{\mathrm{top}} \bar{M}}{100 p}}}, \tag{3}$$

with F-factor $F_{\mathrm{v}}$, relative free area on a tray $\phi$, number of parallel columns $n_{\mathrm{col}}$, ideal gas constant $R$, column top temperature $T_{\mathrm{top}}$, molar mass of the gaseous mixture $\bar{M}$, and column pressure $p$. The values for $F_{\mathrm{v}}$ and $\phi$ are given in ESI Tab. S6.

The column height $H_{\mathrm{col}}$ is determined by the number of trays $N_{\mathrm{col}}$ found by deterministic optimization (simultaneous minimization of OPEX and CAPEX) according to Kossack *et al.*[26] and Kraemer *et al.*[27]. The column height $H_{\mathrm{col}}$ is calculated according to ESI Equation (4):

$$H_{\mathrm{col}} = N_{\mathrm{col}} H_{\mathrm{tray}} + \Delta H, \tag{4}$$

with tray spacing $H_{\mathrm{tray}}$ and extra space $\Delta H$ for the top and bottom of the column. The values for $H_{\mathrm{tray}}$ and $\Delta H$ are given in ESI Tab. S6.

The size of reboiler/condenser heat exchange area $A_{\mathrm{R/C}}$ is calculated according to ESI Equation (5):

$$A_{\mathrm{R/C}} = \frac{\dot{Q}_{\mathrm{R/C}}}{k_{\mathrm{R/C}} T_{\log}}, \tag{5}$$

with heat demand $\dot{Q}_{\mathrm{R/C}}$ of the reboiler or condenser of the column, heat exchange coefficient $k_{\mathrm{R/C}}$, and logarithmic mean temperature difference $T_{\log}$. The values for $k_{\mathrm{R/C}}$ are given in ESI Tab. S6.

The reactor length $L_{\mathrm{reac}}$ and the diameter $D_{\mathrm{reac}}$ are determined by the volume flow $\dot{V}_{\mathrm{reac}}$ through a cylindrical reactor with volume $V_{\mathrm{reac}}$ and residence time $\tau_{\mathrm{reac}}$. The Volume $V_{\mathrm{reac}}$ is calculated through the first equality in ESI Equation (6) and the reactor length $L_{\mathrm{reac}}$ and the diameter $D_{\mathrm{reac}}$ through the second equality in ESI Equation (6) and ESI Equation (7):

$$V_{\mathrm{reac}} = \frac{\dot{V}_{\mathrm{reac}} \tau_{\mathrm{reac}}}{\epsilon} = \frac{\pi}{4} D_{\mathrm{reac}}^2 L_{\mathrm{reac}} \tag{6}$$

$$\frac{L_{\mathrm{reac}}}{D_{\mathrm{reac}}} = 4, \tag{7}$$

with bed voidage $\epsilon$ given in ESI Tab. S6.

Investment costs for compressors and pumps are directly determined by their shaft power.[28]

Table S6: Parameters for column and reactor sizing

| Parameter | Unit | Value | Reference |
|---|---|---|---|
| $F_{\mathrm{v}}$ | $\mathrm{kg}^{0.5}\ \mathrm{m}^{-0.5}\ \mathrm{s}^{-1}$ | 1.4 | Peters and Timmerhaus[29] |
| $\phi$ | – | 0.15 | Peters and Timmerhaus[29] |
| $H_{\mathrm{tray}}$ | m | 0.5 | Peters and Timmerhaus[29] |
| $\Delta H$ | m | 4 | Peters and Timmerhaus[29] |
| $\epsilon$ | – | 0.5 | |
| $k_{\mathrm{R}}$ | $\mathrm{kW\ K^{-1}\ m^{-2}}$ | 0.568 | Luyben[30] |
| $k_{\mathrm{C}}$ | $\mathrm{kW\ K^{-1}\ m^{-2}}$ | 0.852 | Luyben[30] |

The costing of distillation columns, reactors, compressors, and pumps was performed according to the models provided by Guthrie[28]. All column, tray, and heat exchanger cost parameters are taken from the original model. A M&S Index value of 1473.3 (2010) is used. Economic parameters for CAPEX calculations are given in ESI Tab. S7.

Cost of Manufacturing (COM) is calculated according to the procedure given in Turton *et al.*[31]

and can be estimated with ESI Equation (8):[31]

$$\mathrm{COM} = 0.280\mathrm{FCI} + 2.73C_{\mathrm{OL}} + 1.23(C_{\mathrm{UT}} + C_{\mathrm{WT}} + C_{\mathrm{RM}}), \tag{8}$$

with fixed capital investment FCI, cost of operating labor $C_{\mathrm{OL}}$, cost of utilities $C_{\mathrm{UT}}$, cost of waste treatment $C_{\mathrm{WT}}$, and cost of raw materials $C_{\mathrm{RM}}$. ESI Equation (8) is a summation of several cost positions with individual cost parameters listed in Turton *et al.*[31].

Table S7: Economic parameters for CAPEX calculations

| Parameter | Unit | Value |
|---|---|---|
| Plant capacity (w.r.t. DMM) | t $a^{-1}$ | 200000 |
| Interest rate | % | 6 |
| Plant life time | a | 10 |
| Operating hours | hr $a^{-1}$ | 8000 |

## 3.3 Impact on climate change

We forecast the electricity grid mixes for 2030 and 2050 based on the "beyond 2 °C scenario" of the Energy Technology Perspectives by the IEA27.[37] For this, we use the shares of the global energy generation of the IEA for each technology and both years. We model the electricity grid mixes with German generation technologies maintaining consistency between country-specific LCI datasets. We further neglect electricity generation by ocean and others, since its share is negligible (in 2030 $<$ 0.07 % and in 2050 $<$ 1.29 %) and LCI datasets are missing. Carbon capture and storage (CCS) technologies are also included in the "beyond 2 °C scenario" but missing in the LCA database. Thus, we model electricity generation in combination with CCS by combining the conventional technology for electricity generation with the remaining greenhouse gas emissions from the IPPC WGIII AR528[38] instead of the original greenhouse gas emissions.

Table S8: LCA datasets for the evaluation of the reaction pathways for DMM synthesis. Abbreviation: LCIA = Life Cycle Impact Assessment

| Product/utility | Dataset name | Region | Scenario | Comment |
|---|---|---|---|---|
| Hydrogen | PEM electrolysis | N/A | Worst | specific energy consumption = 5.0 kWh $Nm^{-3}$ [32] |
| Hydrogen | SOEC electrolysis | N/A | Best | specific energy consumption = 3.7 kWh $Nm^{-3}$ [32] |
| Hydrogen [a,c] | DE: Hydrogen (steam reforming from natural gas) | DE | N/A | For sensitivity analysis of carbon-intensity of electricity supply only. |
| Carbon dioxide | $CO_2$ from direct air capture | N/A | Worst | von der Assen *et al.*[33] |
| Carbon dioxide | $CO_2$ from ethylene oxide plant | N/A | Best | von der Assen *et al.*[33] |
| Electricity, grid mix [b,c] | Market for electricity, medium voltage, DE | DE | Worst | N/A |
| Electricity, wind onshore [b,c] | Electricity production, wind, 1 MW to 3 MW turbine, onshore, DE | DE | Best | N/A |
| Thermal energy (T<90 °C) [b,c] | Steam production, as energy carrier, in chemical industry, RER | Europe | Worst | N/A |
| Thermal energy (T<90 °C) | Heat pump | N/A | Best | COP = 3.28, averaged from David *et al.*[34], Fig. 3: blue bars with: $T_{source}$ = 9 °C to 15 °C, $T_{operating}$ = 90 °C |
| Thermal energy (90 °C<T<250 °C) [b,c] | Steam production, as energy carrier, in chemical industry, RER | Europe | Worst | N/A |
| Thermal energy (90 °C<T<250 °C) | Electrode boiler | N/A | Best | $\eta = 0.95$ [35] |
| Thermal energy (T>250 °C) [b,c] | Heat production, natural gas, at boiler modulating >100 kW, Europa without Switzerland | Europe | Worst | N/A |
| Thermal energy (90 °C<T<250 °C) | Electrode boiler | N/A | Best | $\eta = 0.95$ [35] |
| Cooling energy | Vapor recompression refrigeration system | N/A | N/A | Estimation via carnot cycle with $\eta_{exergy} = 0.50$ (own assumption), $T_{sink}$ = 25 °C, $T_{cool}$ = −25 °C |
| Process water [b,c] | market for water, deionised, Europe without Switzerland | Europe | N/A | N/A |
| Waste water treatment [b,c] | Treatment of wastewater, average capacity $1 \times 10^9$ $La^{-1}$, Europe without Switzerland | Europe | N/A | N/A |
| Methyl formate [b,c] | Methyl formate production, RER | Europe | N/A | Only relevant if avoided burdens for side products are considered. |
| Dimethyl ether [b,c] | Dimethyl ether production, RER | Europe | N/A | Only relevant if avoided burdens for side products are considered. |

[a] LCA Database: GaBi[36].
[b] LCA Database: ecoinvent 3.6, cut-off.
[c] LCIA Method: ILCD 2.0 midpoint, climate change total.

Table S9: Life Cycle Inventory (LCI) dataset for the electricity supply

| Process | Dataset | Reference |
|---|---|---|
| Wind | EU-28: Electricity from wind power | [36] |
| Norway | NO: Electricity grid mix | [36] |
| France | FR: Electricity grid mix | [36] |
| Photovoltaics [a] | DE: Electricity from photovoltaic | [36] |
| Global 2030 | N/A | cf. ESI Tab. S10 |
| Global 2050 | N/A | cf. ESI Tab. S10 |
| Switzerland | CH: Electricity grid mix | [36] |
| Finland | FI: Electricity grid mix | [36] |
| Denmark | DK: Electricity grid mix | [36] |
| Austria | AT: Electricity grid mix | [36] |
| EU | EU-28: Electricity grid mix | [36] |
| Italy | IT: Electricity grid mix | [36] |
| Germany | DE: Electricity grid mix | [36] |
| USA | CH: Electricity grid mix | [36] |

[a] German dataset is used since an European dataset was not available.

Table S10: Life Cycle Inventory (LCI) for the forecast of the global electricity grid mix in 2030 and 2050 based on the "beyond 2 °C scenario" of the IEA[37]

| Process | Dataset | Share [%] | | Reference |
|---|---|---|---|---|
| | | 2030 | 2050 | |
| Biomass and waste [a] | DE: Electricity from biomass (solid) and DE: Electricity from waste | 6.3 | 8.2 | [36] |
| Biomass CCS [b] | DE: Electricity from biomass (solid) | 0 | 2.7 | N/A |
| Geothermal [c] | IS: Electricity from geothermal | 1.1 | 2.3 | [36] |
| Coal | DE: Electricity from hard coal | 11.3 | 0 | [36] |
| Coal CCS [b] | DE: Electricity from hard coal | 1 | 4.1 | N/A |
| Hydro | DE: Electricity from hydro power | 18.5 | 18.2 | [36] |
| Gas | DE: Electricity from natural gas | 23.8 | 1.5 | [36] |
| Gas CCS [b] | DE: Electricity from natural gas | 0.5 | 4.1 | N/A |
| Nuclear | DE: Electricity from nuclear | 15.4 | 16.2 | [36] |
| Oil | DE: Electricity from heavy fuel oil | 1.3 | 0.2 | [36] |
| Solar [d] | DE: Electricity from photovoltaic | 7.3 | 22.8 | [36] |
| Wind [e] | DE: Electricity from wind power | 13.5 | 19.8 | [36] |

[a] 50 % biomass and 50 % waste.
[b] CCS remaining greenhouse gas emissions:[38] biomass: $0\,g_{CO_2-eq.}\,kWh^{-1}$, coal: $200\,g_{CO_2-eq.}\,kWh^{-1}$, gas: $170\,g_{CO_2-eq.}\,kWh^{-1}$.
[c] Dataset for Germany not available.
[d] Solar includes photovoltaics and concentrated solar power. For both technologies the dataset of photovoltaic is assumed due to the lack of data.
[e] Onshore and offshore.

# 4 Mass and energy balances

Table S11: DMM-specific material input for each pathway and level

| Pathway | Mass [kg kg$^{-1}$] | | | | | |
|---|---|---|---|---|---|---|
| | $H_2$ | | | $CO_2$ | | |
| | L1 | L2 | L3 | L1 | L2 | L3 |
| Established | 0.238 | 0.264 | 0.265 | 1.735 | 1.923 | 1.925 |
| Oxidative | 0.238 | 0.253 | 0.254 | 1.735 | 1.840 | 1.851 |
| Reductive | 0.212 | 0.219 | | 1.735 | 1.791 | |
| Dehydrogenative | 0.212 | 0.258 | | 1.735 | 2.251 | |
| Transfer-hydrogenative | 0.212 | | | 1.735 | | |

Table S12: DMM-specific material output for each pathway and level

| Pathway | Mass [kg kg$^{-1}$] | | | | | | | | | | | |
|---|---|---|---|---|---|---|---|---|---|---|---|---|
| | MF | | | DME | | | $CO_2$ | | | $H_2O$ | | |
| | L1 | L2 | L3 | L1 | L2 | L3 | L1 | L2 | L3 | L1 | L2 | L3 |
| Established | 0.000 | 0.000 | 0.000 | 0.000 | 0.000 | 0.000 | 0.000 | 0.176 | 0.176 | 1.184 | 1.223 | 1.223 |
| Oxidative | 0.000 | 0.000 | 0.000 | 0.000 | 0.005 | 0.007 | 0.000 | 0.057 | 0.058 | 1.184 | 1.219 | 1.224 |
| Reductive | 0.000 | 0.000 | | 0.000 | 0.000 | | 0.000 | 0.042 | | 0.947 | 0.956 | |
| Dehydrogenative | 0.000 | 0.255 | | 0.000 | 0.025 | | 0.000 | 0.078 | | 0.947 | 1.141 | |
| Transfer-hydrogenative | 0.000 | | | 0.000 | | | 0.000 | | | 0.947 | | |

Table S13: DMM-specific energy streams for each pathway and level. Negative values denote outgoing energy streams. Heat integration was performed via pinch analysis

| Pathway | Energy [MJ kg$^{-1}$] | | | | | |
|---|---|---|---|---|---|---|
| | Heat | | | Electricity | | |
| | L1 | L2 | L3 | L1 | L2 | L3 |
| Established | 0.000 | 2.101 (90 °C) | 1.465 (80 °C) | 0.000 | 1.148 | 1.421 |
| Oxidative | 0.000 | 1.545 (58 °C)<br>−0.351 (−25 °C) | −0.161 (1 000 °C)<br>−0.206 (−20 °C) | 0.000 | 2.422 | 2.640 |
| Reductive | 0.000 | 10.949 (86 °C)<br>1.111 (64 °C) | | 0.000 | 1.079 | |
| Dehydrogenative | 0.000 | 23.590 (100 °C) | | 0.000 | 1.739 | |
| Transfer-hydrogenative | 0.000 | | | 0.000 | | |

Table S14: Stoichiometric $H_2$ consumption for the synthesis of various e-fuels from $H_2$ and $CO_2$ relative to their heating values (both LHV and HHV). For DMM synthesis, the non-oxidative pathways are considered. The specific LHV and HHV of fossil diesel is 42.6 MJ kg$^{-1}$ and 45.6 MJ kg$^{-1}$, respectively

| | Unit | DMM | Ethanol | Methanol | DME | Methane |
|---|---|---|---|---|---|---|
| Molar $H_2$ consumption | [mol mol$^{-1}$] | 8 | 6 | 3 | 6 | 4 |
| Molar mass | [g mol$^{-1}$] | 76.1 | 46.1 | 32.0 | 46.1 | 16.0 |
| Specific LHV | [MJ kg$^{-1}$] | 23.3 | 26.7 | 19.9 | 28.9 | 50 |
| Specific HHV | [MJ kg$^{-1}$] | 25.7 | 29.7 | 23.0 | 31.7 | 55.5 |
| Molar LHV | [MJ mol$^{-1}$] | 1.77 | 1.23 | 0.64 | 1.33 | 0.80 |
| Molar HHV | [MJ mol$^{-1}$] | 1.96 | 1.37 | 0.74 | 1.46 | 0.89 |
| $H_2$ consumption/LHV | [mol MJ$^{-1}$] | 4.5 | 4.9 | 4.7 | 4.5 | 5.0 |
| $H_2$ consumption/HHV | [mol MJ$^{-1}$] | 4.1 | 4.4 | 4.1 | 4.1 | 4.5 |

# 5 Production cost

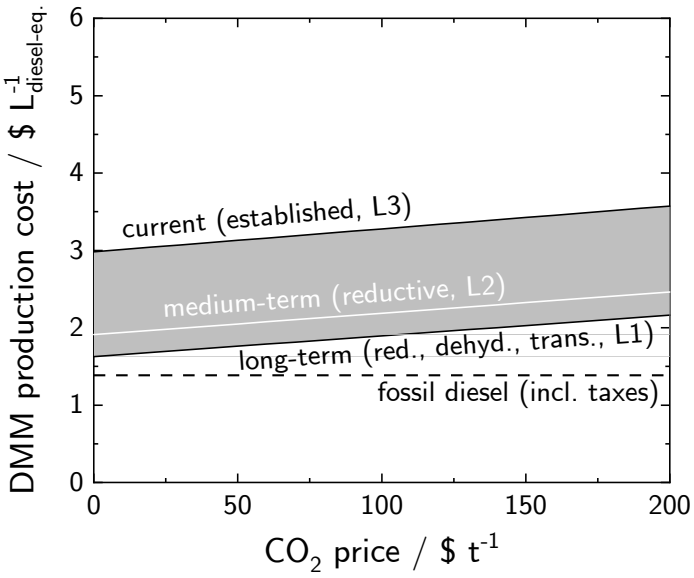


Figure S1: DMM production cost dependence on $CO_2$ price. The base case $H_2$ price is $5\,\$\,kg^{-1}$.[39]

Table S15: Operating (OPEX) and investment (CAPEX) cost for each pathway and level

| Category | Cost [M$ $a^{-1}$] | | | | | | | | | | | | | | |
|---|---|---|---|---|---|---|---|---|---|---|---|---|---|---|---|
| | Established | | | Oxidative | | | Reductive | | | Dehydrogenative | | | Transfer-hydrogenative | | |
| | L1 | L2 | L3 | L1 | L2 | L3 | L1 | L2 | L3 | L1 | L2 | L3 | L1 | L2 | L3 |
| **OPEX** | 262.23 | 296.62 | 314.06 | 262.23 | 310.02 | 307.31 | 235.67 | 273.34 | | 235.67 | 349.06 | | 235.67 | | |
| $H_2$ | 239.04 | 264.97 | 265.34 | 239.04 | 253.54 | 253.57 | 212.48 | 219.92 | | 212.48 | 259.06 | | 212.48 | | |
| $CO_2$ | 23.19 | 25.71 | 25.75 | 23.19 | 24.60 | 24.61 | 23.19 | 23.94 | | 23.19 | 30.10 | | 23.19 | | |
| Heating | | 3.27 | 6.60 | | 2.40 | 0 | | 18.77 | | | 36.71 | | | | |
| Cooling | | 2.66 | 4.30 | | 9.03 | 6.16 | | 1.17 | | | 7.82 | | | | |
| Electricity | | 10.15 | 12.08 | | 21.42 | 22.98 | | 9.54 | | | 15.38 | | | | |
| **CAPEX** | | | 9.26 | | | 4.08 | | | | | | | | | |
| Columns | | | 7.16 | | | 2.80 | | | | | | | | | |
| Reactors | | | 0.11 | | | 0.06 | | | | | | | | | |
| Pumps | | | 0.01 | | | 0.02 | | | | | | | | | |
| Compressors | | | 1.99 | | | 1.21 | | | | | | | | | |

Table S16: Cost of Manufacturing (COM) for the established and oxidative pathway on Level 3

| Category | Cost [M\$ $a^{-1}$] | |
|---|---|---|
| | Established pathway | Oxidative pathway |
| **Direct Manufacturing Costs (DMC)** | 333.19 | 322.08 |
| Raw materials ($C_{\mathrm{RM}}$) | 291.09 | 278.18 |
| Waste treatment ($C_{\mathrm{WT}}$) | 0 | 0 |
| Utilities ($C_{\mathrm{UT}}$) | 22.98 | 29.14 |
| Operating labor ($C_{\mathrm{OL}}$) | 1.60 | 0.78 |
| Direct supervisory and clerical labor | 0.29 | 0.14 |
| Maintenance and repairs | 4.09 | 1.80 |
| Operating supplies | 0.61 | 0.27 |
| Laboratory charges | 0.24 | 0.17 |
| Patents and royalities | 12.29 | 11.66 |
| **Fixed Manufacturing Costs (FMC)** | 15.04 | 6.68 |
| Depreciation | 9.26 | 4.08 |
| Local taxes and insurances | 2.18 | 0.96 |
| Plant overhead costs | 3.59 | 1.63 |
| **General Manufacturing Costs (GM)** | 66.46 | 62.57 |
| Administration costs | 0.90 | 0.41 |
| Distribution and selling costs | 45.07 | 42.74 |
| Research and development | 20.49 | 19.43 |
| **Total costs** | 414.69 | 391.33 |
| Total costs in $\left[\$\,\mathrm{L}^{-1}_{\text{diesel-eq.}}\right]$ | 3.19 | 3.02 |

# 6 Impact on climate change

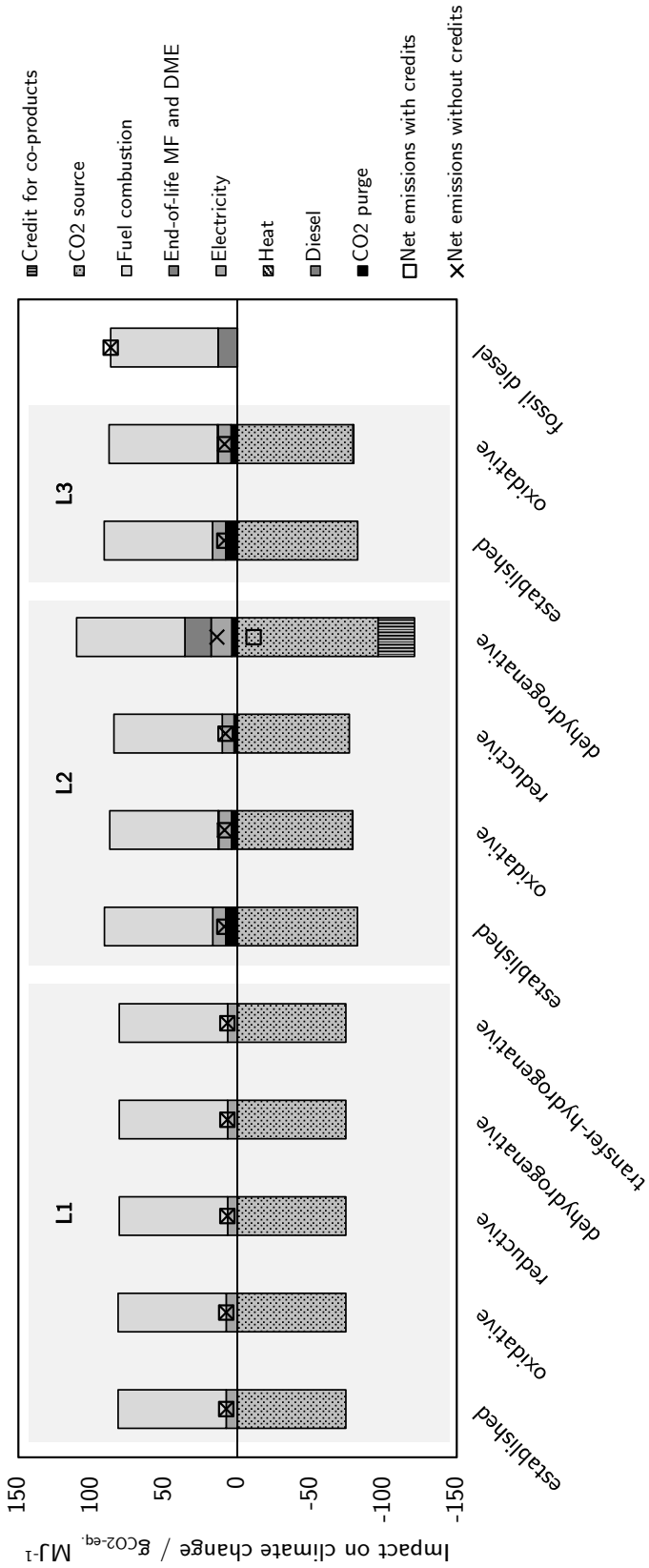


Figure S2: Contribution analysis of the cradle-to-grave impact on climate change of different DMM synthesis pathways per MJ fuel evaluated on different levels and compared to fossil diesel for the best case scenario. The functional unit is "the provision of 1 MJ of enthalpy of combustion". In the best case scenario, $CO_2$ is provided by an ideal industrial point source and hydrogen is produced by an SOEC. Electricity is supplied by a German onshore wind turbine, while heat is supplied by heat pump and electrode boiler for temperature levels of up to 90 °C and above 90 °C, respectively. Cooling energy is provided by a vapor compression refrigeration system. $CO_2$ otherwise emitted by the ideal point source is negative and reemitted during fuel combustion. The combustion of the co-products MF and DME at their end-of-life is included for the dehydrogenative and oxidative pathway on Level 2 and 3 to cover the cradle-to-grave perspective. If credits for excess heat and MF and DME co-production is given, cradle-to-grave $CO_2$ emissions for the dehydrogenative pathway reach a negative value ($-11\,g_{CO_2-eq.}\,MJ^{-1}$). This negative value does not imply a removal of $CO_2$ emissions from the atmosphere, but rather reflect that the life cycles of MF and DME become environmentally more beneficial if co-produced with DMM compared to their conventional production.

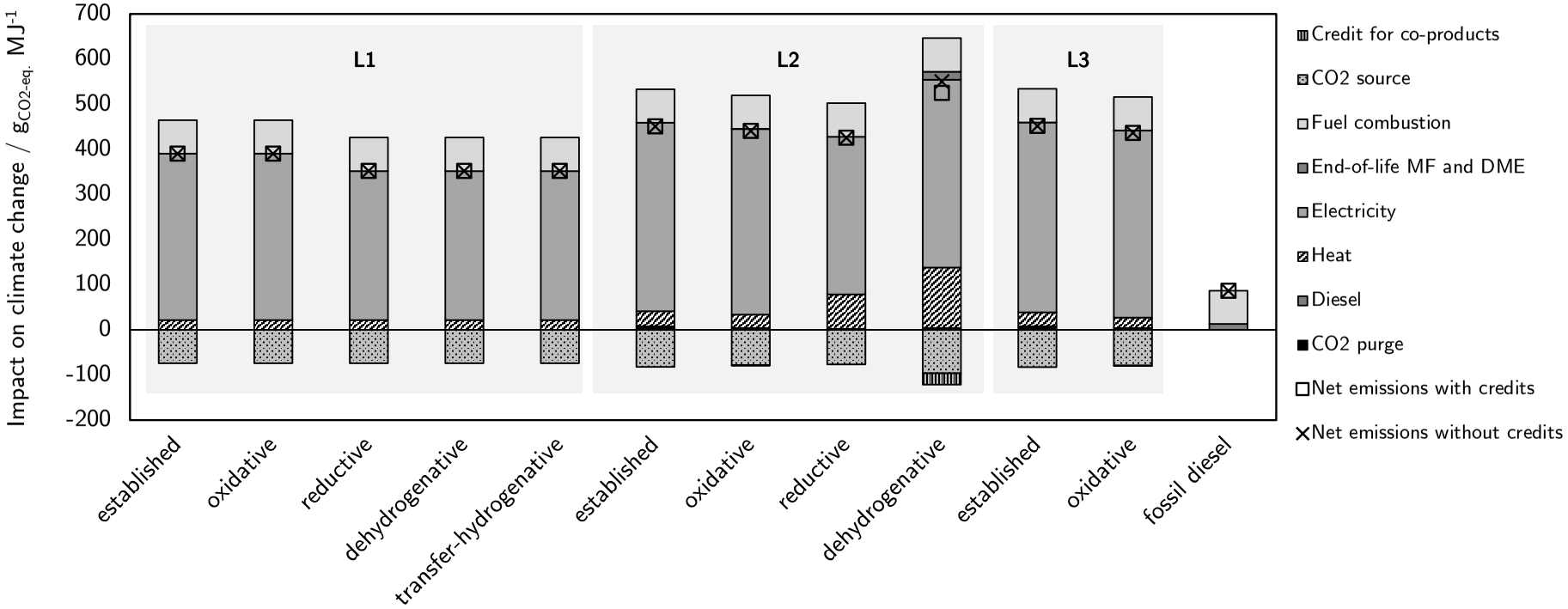


Figure S3: Contribution analysis of the cradle-to-grave impact on climate change of different DMM synthesis routes per MJ fuel evaluated on different levels and compared to fossil diesel for the worst case scenario. The functional unit is "the provision of 1 MJ of enthalpy of combustion". In the worst case scenario, $CO_2$ is provided by direct air capture and hydrogen is produced by a PEM electrolysis. Electricity is supplied by todays power grid mix of Germany, while heat is supplied by steam and an NG-boiler for temperature levels of up to 250 °C and above 250 °C, respectively. Cooling energy is provided by a vapor compression refrigeration system. $CO_2$ removed from air by direct air capture is negative and reemitted during fuel combustion. The combustion of the co-products MF and DME at their end-of-life is included for the dehydrogenative and oxidative pathway on Level 2 and 3 to cover the cradle-to-grave perspective.

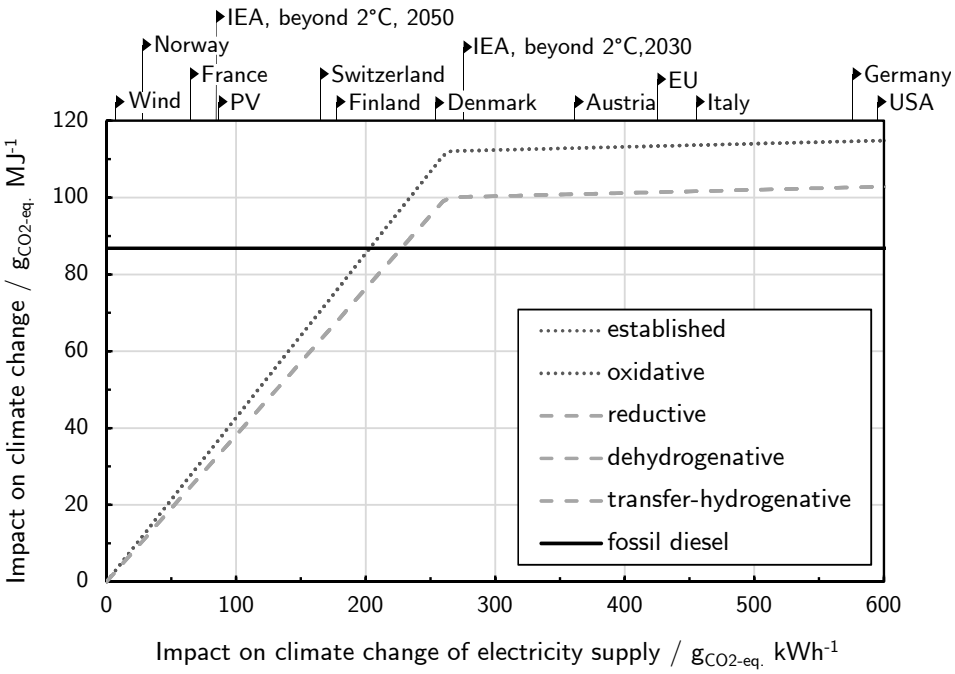


Figure S4: Sensitivity of the cradle-to-grave impact on climate change of DMM with respect to the impact on climate change of electricity supply for different DMM synthesis pathways on Level 1 and fossil diesel. The impact on climate change is calculated using the stoichiometric mass balances of each pathway. $H_2$ is supplied by SOEC instead of conventional steam methane reforming below $260\,g_{CO_2-eq.}\,kWh^{-1}$. The solid black lines at the top of the graph represent the impact on climate change of country-specific grid mixes and two forecasts for the global grid mix of 2030 and 2050 that are based on the "beyond 2 °C scenario" of the International Energy Agency.[37] The dotted gray lines (established and oxidative) are on top of each other and the dashed gray lines (reductive, dehydrogenative, and transfer-hydrogenative) are on top of each other.

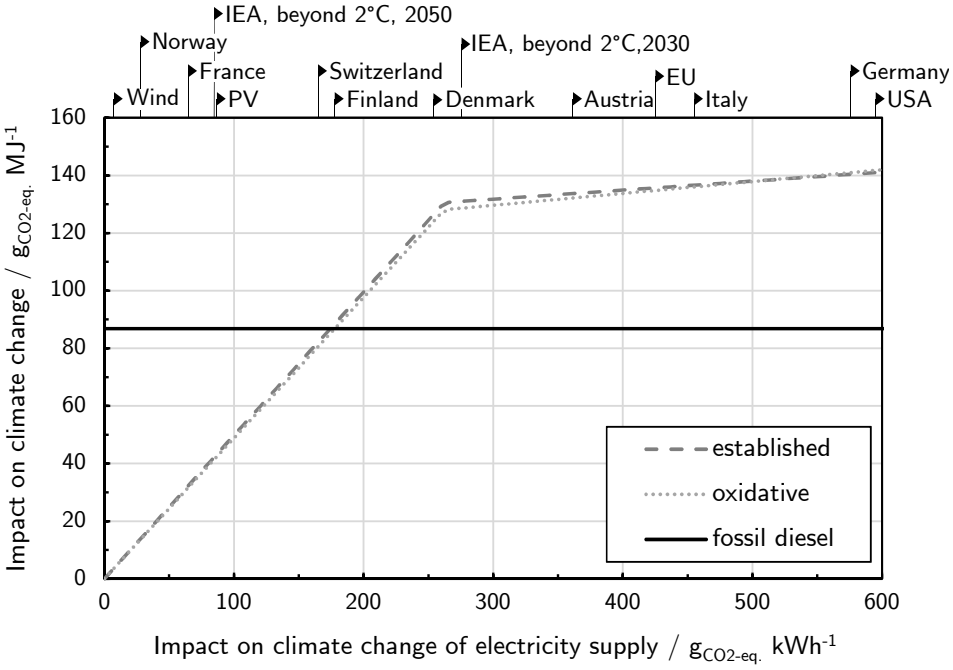


Figure S5: Sensitivity of the cradle-to-grave impact on climate change of DMM with respect to the impact on climate change of electricity supply for different DMM synthesis pathways on Level 3 and fossil diesel. The impact on climate change is calculated using the current catalyst performance of each pathway. Avoided burdens for co-produced side products and excess heat are not considered. $H_2$ is supplied by SOEC instead of conventional steam methane reforming below 260 $g_{CO_2-eq.}$ $kWh^{-1}$. The solid black lines at the top of the graph represent the impact on climate change of country-specific grid mixes and two forecasts for the global grid mix of 2030 and 2050 that are based on the "beyond 2 °C scenario" of the International Energy Agency.[37]

# 7 Pathway potential at equilibrium conditions

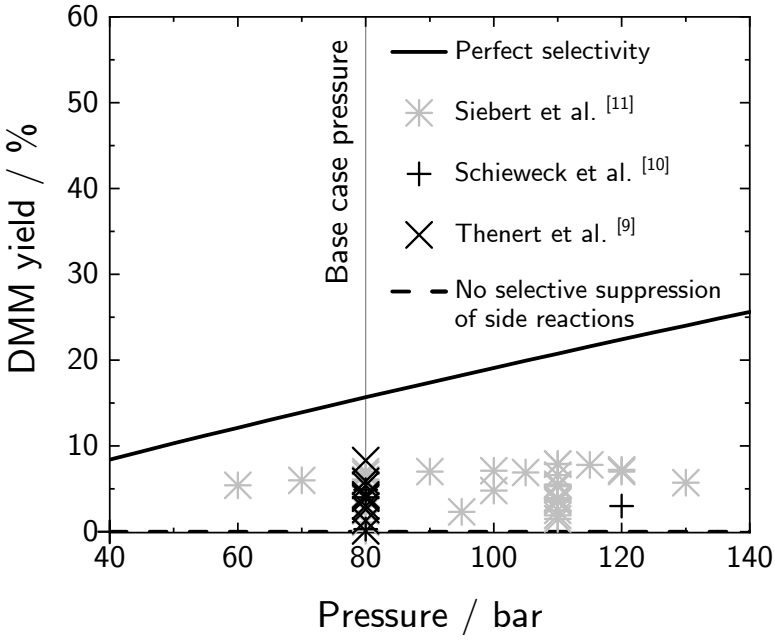


Figure S6: DMM yield dependence on reactor pressure for the reductive pathway (cf. Reaction (R6)). Restricted equilibrium conversion (considering perfect DMM selectivity) has been considered throughout the entire pressure range. Equilibrium conversion was calculated with an REquil reactor model in Aspen Plus v11. For the 'No selective suppression of side reactions' case additional DME and carbon monoxide (CO) formation was considered.

Table S17: DMM-specific material and energy balances for each pathway at equilibrium conversion and perfect selectivity on Level 2. Negative values denote outgoing energy streams. Heat integration was performed via pinch analysis

| Pathway | Mass [kg kg$^{-1}$] | | | | | | Energy [MJ kg$^{-1}$] | |
|---|---|---|---|---|---|---|---|---|
| | Input | | Output | | | | | |
| | $H_2$ | $CO_2$ | MF | DME | $CO_2$ | $H_2O$ | Heat | Electricity |
| Reductive | 0.218 | 1.780 | 0.000 | 0.000 | 0.039 | 0.953 | 1.491 (100 °C)<br>0.802 (58 °C) | 1.072 |
| Dehydrogenative | 0.223 | 1.819 | 0.001 | 0.000 | 0.057 | 0.968 | 5.823 (100 °C) | 1.327 |
| Transfer-hydrogenative without $H_2$ recycling | 0.248 | 1.804 | 0.000 | 0.000 | 0.056 | 0.945 | −1.256 (230 °C) | 1.076 |
| Transfer-hydrogenative with $H_2$ recycling | 0.221 | 1.804 | 0.000 | 0.000 | 0.056 | 0.945 | 0.476 (78 °C)<br>9.764 (630 °C) | 1.268 |
| Transfer-hydrogenative with $H_2$ recycling at no cost | 0.221 | 1.804 | 0.000 | 0.000 | 0.056 | 0.945 | −1.256 (230 °C) | 1.268 |

## 7.1 Potential pathway improvements

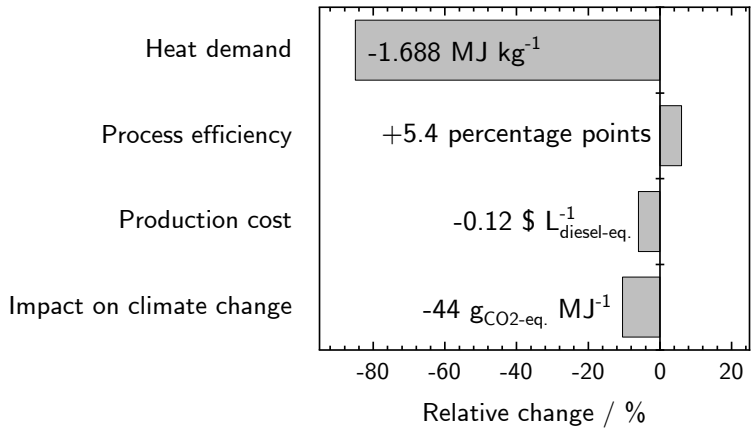


Figure S7: Potential improvements of the reductive pathway if restricted equilibrium methanol conversion (15.7 %) instead of experimental conversion (10.1 %) and perfect DMM selectivity instead of experimental selectivity (81.8 %) at a reaction temperature of 80 °C is assumed. The results on impact on climate change are given for the worst case scenario.

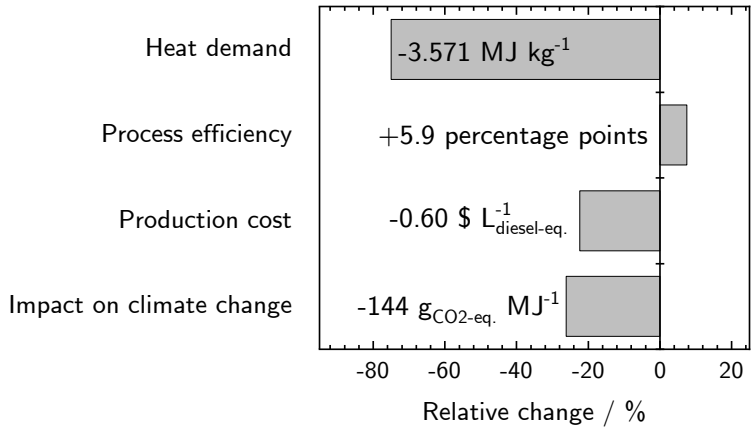


Figure S8: Potential improvements of the dehydrogenative pathway if restricted equilibrium methanol conversion (9.8 %) at 300 °C instead of the experimental conversion (3.6 %) at 200 °C and perfect DMM selectivity instead of experimental selectivity (80.3 %) is assumed. The results on impact on climate change are given for the worst case scenario.

## 7.2 Impact on climate change

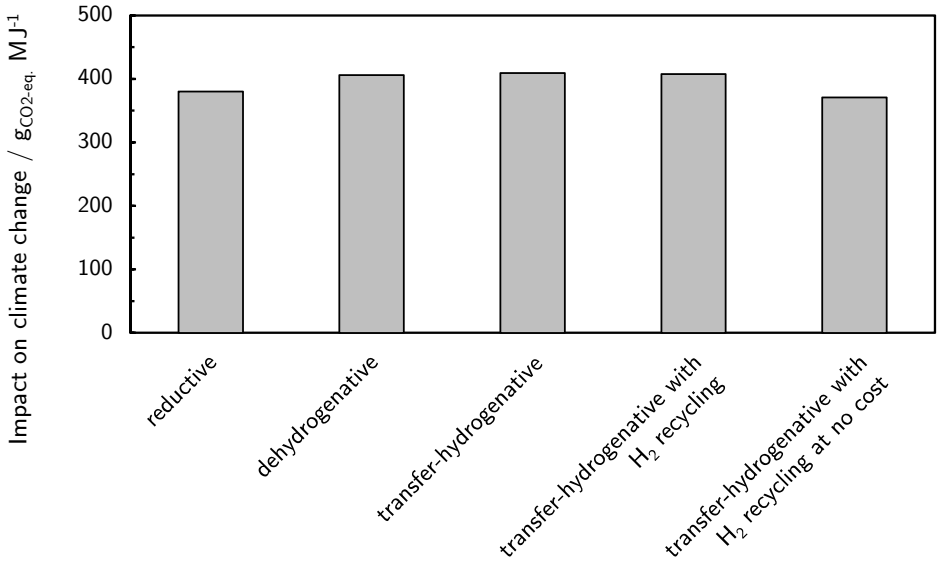


Figure S9: Cradle-to-grave impact on climate change for the worst case scenario of DMM synthesis via the reductive, dehydrogenative, and three variations of the transfer-hydrogenative route at Level 2 with perfect selectivity and equilibrium conversion. Avoided burdens for excess heat and co-production of MF are not considered. The functional unit is "the provision of 1 MJ of enthalpy of combustion".

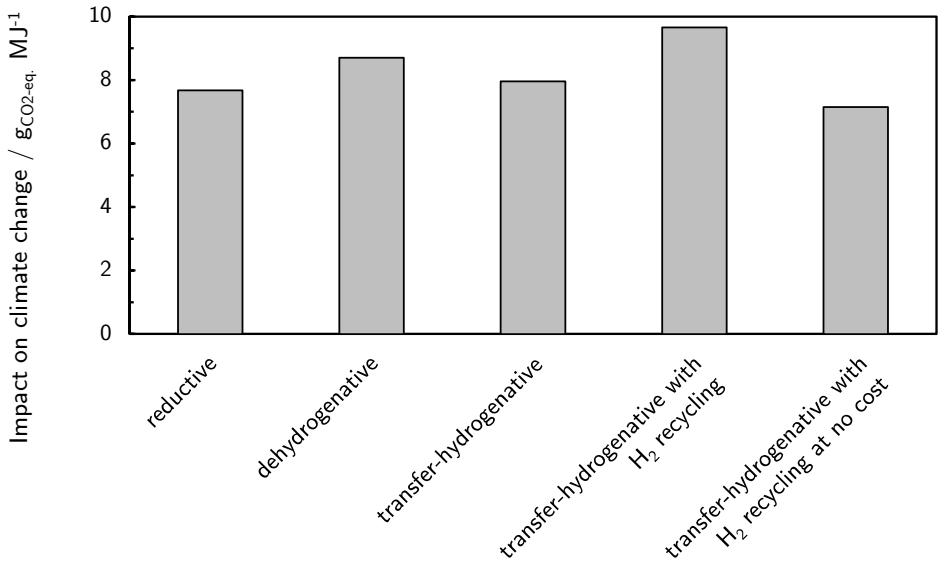


Figure S10: Cradle-to-grave impact on climate change for the best case scenario of DMM synthesis via the reductive, dehydrogenative, and three variations of the transfer-hydrogenative pathway at Level 2 with perfect selectivity and equilibrium conversion. Avoided burdens for excess heat and co-production of MF are not considered. The functional unit is "the provision of 1 MJ of enthalpy of combustion".

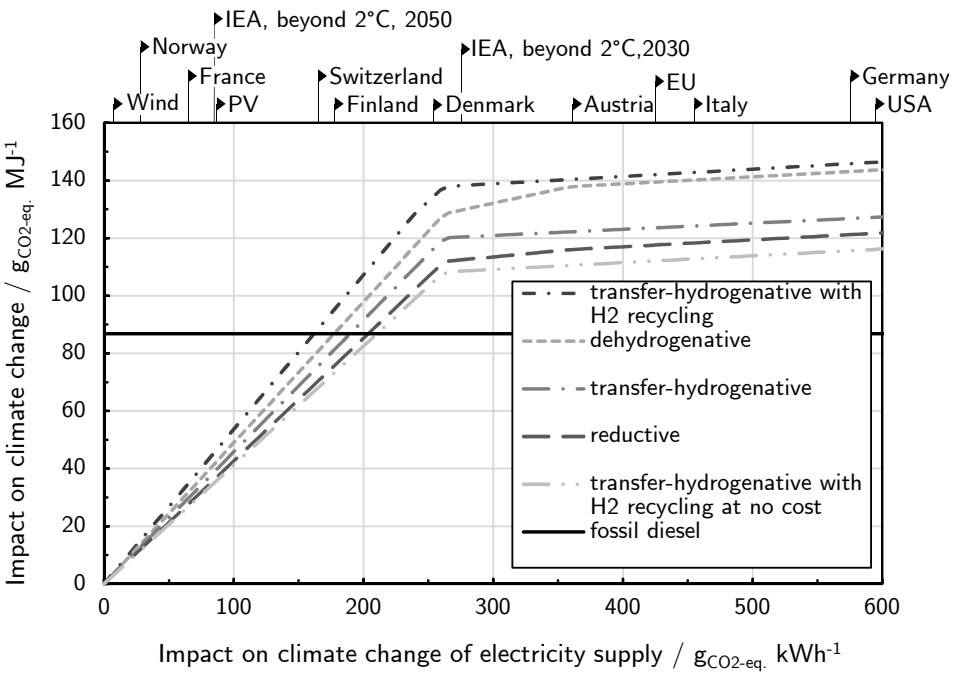


Figure S11: Sensitivity of the cradle-to-grave impact on climate change of DMM with respect to the impact on climate change of electricity supply for different DMM synthesis pathways on Level 2 and fossil diesel. The impact on climate change is calculated considering equilibrium conversion and perfect selectivity of each pathway. $H_2$ is supplied by SOEC instead of conventional steam methane reforming below $260\,g_{CO_2-eq.}\,kWh^{-1}$. The solid black lines at the top of the graph represent the impact on climate change of country-specific grid mixes and two forecasts for the global grid mix of 2030 and 2050 that are based on the "beyond 2 °C scenario" of the International Energy Agency.[37]

## 7.3 Maximum potential of non-oxidative pathways

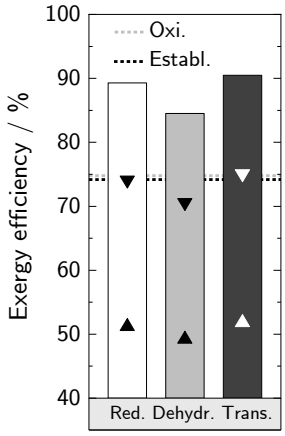


(a) Exergy efficiency of the DMM synthesis routes from $H_2$ and $CO_2$ (bars) and for the entire system for the worst (▲) and best (▼) case scenario. The dashed lines correspond to the established and oxidative pathway evaluated on Level 2 considering actual reaction performance.

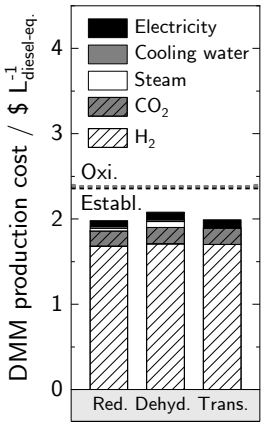


(b) Cost of DMM production. The dashed lines correspond to the established and oxidative pathway evaluated on Level 2 considering actual reaction performance.

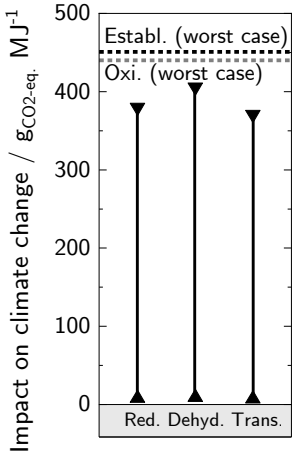


(c) Impact of DMM on climate change for the worst (▼) and best (▲) case scenario. The dashed lines correspond to the worst case scenario for the established and oxidative pathway evaluated on Level 2 considering actual reaction performance.

Figure S12: Exergy efficiency (ESI Fig. S12a), production cost (ESI Fig. S12b), and impact on climate change (ESI Fig. S12c) for DMM production via the reductive, dehydrogenative, and transfer-hydrogenative synthesis route considering perfect selectivity and equilibrium conversion evaluated on Level 2. For the transfer-hydrogenation, EB dehydrogenation at no cost has been considered.

# 8 Process flowsheets

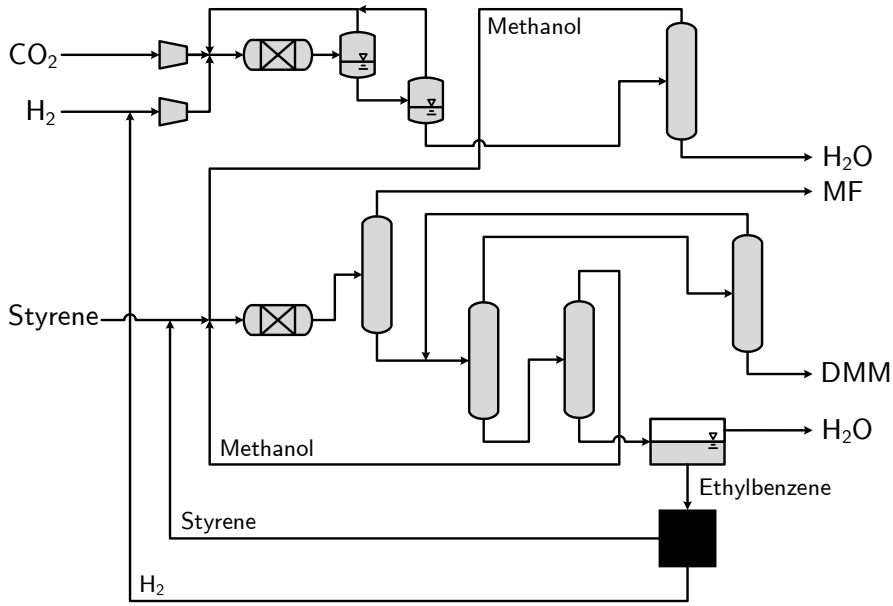


Figure S13: Process concept for the transfer-hydrogenative pathway on Level 2. All possible distillation sequences have been screened and the least energy-intensive sequence has been chosen. Styrene is added to the reactor in such a way that it is completely converted to EB and simultaneously consumes co-produced $H_2$ completely. Modeling detail is identical to that of the alternative non-oxidative pathways with the process step for EB dehydrogenation as an exception. Ethylbenzene dehydrogenation is modeled as a black box with process parameters at equilibrium conditions from the literature.[40]

# 9 Future research directions

Table S18: Bottlenecks of each reaction pathway, their impact on key performance indicators, and potential measures for improvements

| Reaction Pathways | Bottlenecks | Impact on KPIs | Improvement measures |
|---|---|---|---|
| Established | High $H_2$ consumption due to oxidative FA production | High | FA prod. via methanol dehydrogenation |
| | Three process steps | Low | none[a] |
| Oxidative | High $H_2$ consumption due to oxidative in-situ FA formation | High | none[a] |
| | High DMM dilution in reactor effluent | Medium | Pure oxygen as oxidant and methanol excess |
| | High cooling demand | Medium | Application of an alternative gas separation |
| Reductive | Gap to chemical equilibrium | Medium | Further catalyst optimization to suppress catalyst deactivation |
| Dehydrogenative | Low equilibrium conversion | High | In-situ $H_2$ removal (e.g., by membrane reactor) |
| | Comparatively low DMM selectivity | Medium | Further catalyst optimization to suppress side reactions |
| | Gas separation for $H_2$ recycling necessary | Medium | none[a] |
| Transfer-hydrogenative | Gap to chemical equilibrium | High | Further catalyst optimization to suppress catalyst deactivation |
| | Currently only model substrate as hydrogen carrier | High | Extending the reaction to use industrially viable hydrogen acceptors |

[a] Intrinsically given by reaction pathway.

**Acknowledgments** The authors gratefully acknowledge funding by the German Federal Ministry of Education and Research (BMBF) within the Kopernikus Project P2X: Flexible use of renewable resources – exploration, validation and implementation of "Power-to-X" concepts (FKZ 03SFK2A) and the project NAMOSYN: Nachhaltige Mobilität durch synthetische Kraftstoffe (FKZ 03SF0566P0). This work is further funded by Deutsche Forschungsgesellschaft (DFG, German Research Foundation) under Germany's Excellence Strategy – Cluster of Excellence 2186 "The Fuel Science Center" – ID: 390919832.

# References

[1] J.-O. Weidert, J. Burger, M. Renner, S. Blagov and H. Hasse, *Industrial & Engineering Chemistry Research*, 2017, **56**, 575–582.

[2] W. Wang, S. Wang, X. Ma and J. Gong, *Chemical Society Reviews*, 2011, **40**, 3703.

[3] É. S. Van-Dal and C. Bouallou, *Journal of Cleaner Production*, 2013, **57**, 38–45.

[4] M. Pérez-Fortes, J. C. Schöneberger, A. Boulamanti and E. Tzimas, *Applied Energy*, 2016, **161**, 718–732.

[5] O.-S. Joo, K.-D. Jung, I. Moon, A. Y. Rozovskii, G. I. Lin, S.-H. Han and S.-J. Uhm, *Industrial & Engineering Chemistry Research*, 1999, **38**, 1808–1812.

[6] G. Reuss, W. Disteldorf, A. Gamer and A. Hilt, *Formaldehyde*, Ullmann's Encyclopedia of Industrial Chemistry, 2000.

[7] R. Sun, I. Delidovich and R. Palkovits, *ACS Catalysis*, 2019, **9**, 1298–1318.

[8] Z. Fan, H. Guo, K. Fang and Y. Sun, *RSC Advances*, 2015, **5**, 24795–24802.

[9] K. Thenert, K. Beydoun, J. Wiesenthal, W. Leitner and J. Klankermayer, *Angewandte Chemie*, 2016, **128**, 12454–12457.

[10] B. G. Schieweck and J. Klankermayer, *Angewandte Chemie*, 2017, **129**, 10994–10997.

[11] M. Siebert, M. Seibicke, A. F. Siegle, S. Kräh and O. Trapp, *Journal of the American Chemical Society*, 2019, **141**, 334–341.

[12] R. Sun, C. Mebrahtu, J. P. Hofmann, D. Bongartz, J. Burre, C. H. Gierlich, P. J. Hausoul, A. Mitsos and R. Palkovits, *Sustainable Energy and Fuels*, in press.

[13] O. Osterthun and J. Klankermayer, *Angewandte Chemie*, submitted.

[14] D. Bongartz, J. Burre and A. Mitsos, *Industrial & Engineering Chemistry Research*, 2019, **58**, 4881–4889.

[15] A. Fredenslund, R. L. Jones and J. M. Prausnitz, *AIChE Journal*, 1975, **21**, 1086–1099.

[16] G. Maurer, *AIChE Journal*, 1986, **32**, 932–948.

[17] H. Hasse, I. Hahnenstein and G. Maurer, *AIChE Journal*, 1990, **36**, 1807–1814.

[18] I. Hahnenstein, H. Hasse, C. G. Kreiter and G. Maurer, *Industrial & Engineering Chemistry Research*, 1994, **33**, 1022–1029.

[19] M. Albert, B. C. García, C. Kreiter and G. Maurer, *AIChE Journal*, 1999, **45**, 2024–2033.

[20] M. Albert, B. C. García, C. Kuhnert, R. Peschla and G. Maurer, *AIChE Journal*, 2000, **46**, 1676–1687.

[21] M. Albert, I. Hahnenstein, H. Hasse and G. Maurer, *Journal of Chemical & Engineering Data*, 2001, **46**, 897–903.

[22] C. Kuhnert, M. Albert, S. Breyer, I. Hahnenstein, H. Hasse and G. Maurer, *Industrial & Engineering Chemistry Research*, 2006, **45**, 5155–5164.

[23] C. B. Dirk-Faitakis, W. An, T.-B. Lin and K. T. Chuang, *Chemical Engineering and Processing: Process Intensification*, 2009, **48**, 1080–1087.

[24] C. F. Breitkreuz, N. Schmitz, E. Ströfer, J. Burger and H. Hasse, *Chemie Ingenieur Technik*, 2018, **90**, 1489–1496.

[25] S. Deutz, D. Bongartz, B. Heuser, A. Kätelhön, L. S. Langenhorst, A. Omari, M. Walters, J. Klankermayer, W. Leitner, A. Mitsos, S. Pischinger and A. Bardow, *Energy & Environmental Science*, 2018, **11**, 331–343.

[26] S. Kossack, K. Kraemer and W. Marquardt, *Industrial & Engineering Chemistry Research*, 2006, **45**, 8492–8502.

[27] K. Kraemer, S. Kossack and W. Marquardt, *Industrial & Engineering Chemistry Research*, 2009, **48**, 6749–6764.

[28] K. M. Guthrie, *Chem. Engng.*, 1969, **24**, 114–142.

[29] M. S. Peters and K. D. Timmerhaus, *Plant design and economics for chemical engineers*, McGraw-Hill, Inc., 1980.

[30] W. L. Luyben, *AIChE Journal*, 2010, **57**, 655–670.

[31] R. Turton, R. C. Bailie, W. B. Whiting and J. A. Shaeiwitz, *Analysis, synthesis and design of chemical processes*, Pearson Education, 2008.

[32] A. Buttler and H. Spliethoff, *Renewable and Sustainable Energy Reviews*, 2018, **82**, 2440–2454.

[33] N. von der Assen, L. J. Müller, A. Steingrube, P. Voll and A. Bardow, *Environmental Science & Technology*, 2016, **50**, 1093–1101.

[34] A. David, B. V. Mathiesen, H. Averfalk, S. Werner and H. Lund, *Energies*, 2017, **10**, 578.

[35] L. J. Müller, A. Kätelhön, M. Bachmann, A. Zimmermann, A. Sternberg and A. Bardow, *Frontiers in Energy Research*, 2020, **8**, 15.

[36] thinkstep AG, *GaBi 9.2.0.58: Software-System and Database for Life Cycle Engineering, DB 8.7 - SP 39*, 2019, Leinfelden-Echterdingen, Germany.

[37] IEA, International Energy Agency, *Energy Technology Perspectives 2017: Catalysing Energy Technology Transformation*, 2017.

[38] IPPC, The Intergovernmental Panel on Climate Change, *Climate change 2014: Working Group III Contribution to the Fifth Assessment Report of the Intergovernmental Panel on Climate Change*, 2014, Cambridge University Press.

[39] T. Grube, L. Doré, A. Hoffrichter, L. E. Hombach, S. Raths, M. Robinius, M. Nobis, S. Schiebahn, V. Tietze, A. Schnettler, G. Walther and D. Stolten, *Sustainable Energy & Fuels*, 2018, **2**, 1500–1515.

[40] N. Mimura and M. Saito, *Catalysis Today*, 2000, **55**, 173–178.